Observation of superfluorescent emissions from laser-cooled atoms

E. Paradis, B. Barrett, and A. Kumarakrishnan
Department of Physics and Astronomy, York University Toronto, ON M3J 1P3 Toronto, Canada

R. Zhang and G. Raithel
Department of Physics, University of Michigan, Ann Arbor, Michigan 48109, USA
(Received 12 November 2007; published 25 April 2008)

We study superfluorescence (SF) from spherical and cigar-shaped clouds of laser-cooled Rubidium atoms from the $5D_{5/2}$ level through the $6P_{3/2}$ level to the $5S_{1/2}$ ground level. The atomic system is initially excited to the $5D_{5/2}$ level from the ground state via two-photon excitation through the intermediate $5P_{3/2}$ level. The fluorescence on the $6P$-$5S$ transition at 420 nm is recorded using time-resolved measurements. The time delays of the observed SF emission peaks typically scale as $\sim N^{-1}$, where N is the atom number, and are much smaller than the time delay expected for uncorrelated cascade fluorescence. Since N is significantly smaller than the threshold number for SF on the 420 nm transition, and larger than the threshold number for the $5D$-$6P$ transition at 5.2 μm, our observations suggest that the 420 nm SF emission is triggered by rapid deexcitation of the $5D$ to the $6P$ level via SF at 5.2 μm. The observed SF time delays for 420 nm emission agree with SF time-delay estimates for the 5.2 μm transition. For spherical clouds, the SF is isotropic. For cigar-shaped clouds, the SF is highly anisotropic. Along the long axis of cigar-shaped atom clouds, SF and incoherent cascade fluorescence produce temporally well-resolved peaks in the detected signal. In this case, the SF component of the signal is highly concentrated along a direction in between the directions of the two almost parallel excitation beams. The observed SF intensities scale as N, suggesting that the $5D$ level is regeneratively pumped during the SF decay.

DOI: 10.1103/PhysRevA.77.043419 PACS number(s): 37.10.De, 42.50.Md, 37.10.Vz, 42.50.Nn

I. INTRODUCTION

Superfluorescence (SF) refers to the evolution of coherent emission from a system of incoherently excited atoms [1]. The coherence evolves from spontaneous emission, and is characterized by a burst of radiation that has some of the features of radiation from a phased array of dipoles [2]. In the ideal case, the peak intensity scales as N_{ex}^2, where N_{ex} is the number of excited atoms, and the pulse width scales as N_{ex}^{-1} to conserve energy. SF is also characterized by a delay time with respect to the excitation pulse. The peak heights, pulse widths, and delay times exhibit fluctuations that can be attributed to the quantum initiation of this process [3,4]. For this reason, SF has been extensively studied as an amplifier of quantum noise [5]. SF differs from super-radiance [6] (SR) in that the direction along which the emission is amplified is determined by the shape of the sample. For SR it is determined by the initial phases of the excitation pulse(s) and phase-matching conditions [7]. SF has been extensively studied in atomic gases to understand its scaling laws [8], effects of pulse propagation [9], quantum fluctuations [1,10,11], and dephasing processes [12,13].

The delay time τ_d for SF is on the same order as the dipole coupling time τ_r, where $\tau_r=(N_{\mathrm{ex}}\Gamma\mu)^{-1}$ is the time in which the collective dipole moment of the system becomes macroscopic [14]. Here, Γ is the rate of spontaneous emission for a single atom and μ is the diffraction solid angle at the SF wavelength. The value of μ is related to the fraction of spontaneously emitted photons that are amplified in a macroscopic medium. For a sphere $[\mu=2\lambda^2/(5\pi A)]$, the SF can be expected to occur in a random direction for every realization, whereas in the case of a cylinder $[\mu=3\lambda^2/(8\pi A)]$ emissions along the long axis can be expected to dominate [2]. Here A represents the cross-sectional area of the excitation region and λ is the wavelength of the SF transition. The threshold number of atoms N_T required for SF is achieved when $\tau_r=T_2$, where T_2 is the dephasing time of the system. For a Doppler-broadened vapor $N_T\sim 10^{10}$ [8], whereas it is typically $\sim 10^5$ for the case of laser-cooled atoms. In the latter case, the effect of Doppler broadening is negligible since typically the Doppler-broadened linewidth is $\Gamma_D \lesssim 1$ MHz, and SF can become a dominant pathway for relaxation. Even for N_{ex} as small as $\sim 10^5$, observations of SF from atom traps can be recorded with a high signal to noise ratio, and studies of SF scaling laws can serve as useful diagnostic tools for studying various dephasing processes, such as cold Rydberg atom interactions [1]. Another interesting aspect of working with atom traps is that it is relatively straightforward to change the shape of the sample and to observe the enhancement of SF along the preferred axes of the atomic cloud.

A fully quantum-mechanical model for SF initiation predicts that the delay time for SF with respect to the excitation pulse is given by [15]

$$\tau_d = \frac{\tau_r}{4}[\ln(\sqrt{2\pi N_{\mathrm{ex}}})]^2. \tag{1}$$

Since τ_d is proportional to τ_r, it approximately scales as N_{ex}^{-1} for pure SF. For Eq. (1) to apply, the propagation (or escape) time for light to travel through the medium τ_e must satisfy $\tau_e < \tau_r$. If $\tau_e > \tau_r$, the emission of the system can be regarded as the incoherent sum of coherent emissions from a number of subregions within the sample that evolve independently

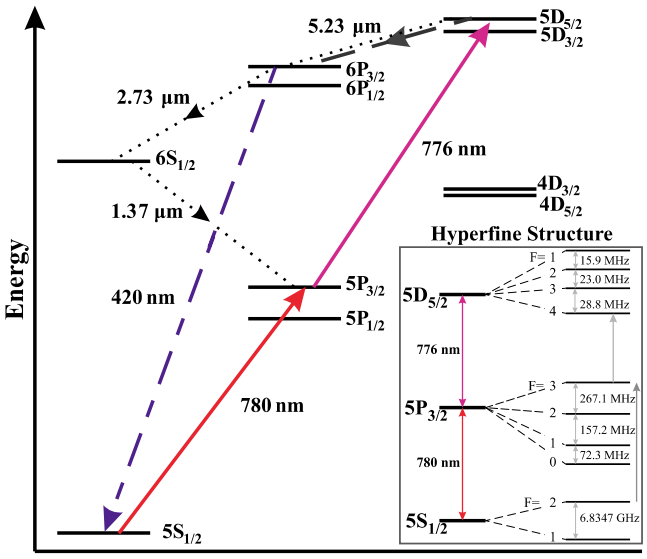

FIG. 1. (Color online) Rubidium 87 level diagram: the solid lines represent excitation pulses, and the dashed lines correspond to SF emissions pertaining to this work. The dotted lines represent the expected SF cascade for incoherent excitation. The radiative lifetimes of the $5D_{5/2} \rightarrow 6P_{3/2}$, $6P_{3/2} \rightarrow 5S_{1/2}$ transitions are 690 and 357 ns, respectively. The total radiative lifetimes of the $5D_{5/2}$ and $6P_{3/2}$ states are 241 and 109 ns, respectively.

[1,16–18]. Apart from realizing the threshold atom number within the coherently evolving (sub)regions, in order to observe SF it is further necessary that $\tau_d < \tau_n$, where τ_n is the natural radiative decay time associated with the excited state. In some cases [18], effects such as radiation trapping can extend the effective lifetime of the excited state. However, radiation trapping does not influence the results discussed in this paper, as discussed in detail near the end of Sec. IV C.

II. PREVIOUS WORK

Previous work, and this study, has been performed on Rb gases. For reference, in Fig. 1 we show the energy level diagram of ^{87}Rb. The transition wavelengths shown in the figure and the lifetimes quoted in the caption are based on Refs. [19,20]. The hyperfine structure of the $5D$ state shown in the inset was measured in Ref. [21] using two-photon spectroscopy. The properties of SF depend critically on whether the excitation is coherent or incoherent. In a previous experiment in atomic Rb vapor, SF was observed [22] in the $5S$-$6P$-$6S$ three-level system (levels shown in Fig. 1). The $5S$-$6P$ transition was excited, and SF was detected on the 2.7 μm $6P$-$6S$ transition. Even for this configuration, care must be taken to avoid any initial coherence due to the pump pulse, since Ref. [23] has shown that avoiding coherent excitation imposes a particularly restrictive condition on pumping.

If this system can be excited without any initial coherence between the $5S$ and $5D$ states, the system can be expected to decay through a multistep SF cascade involving the $6P$-$6S$ (2.7 μm) and $6S$-$5P$ (1.3 μm) transitions. In contrast, if there is an initial coherence between the $5S$ and $5D$ states, the system is expected to decay through SF on the $5D$-$6P$ (5.2 μm) transition and triggered SF on the $6P$-$5S$ (420 nm) transition [24,25]. Examples of triggered SF include Refs. [24–26], which were carried out in Cs and Rb atomic vapors, with ground-state densities of the order of $10^{13}-10^{15}$ cm^{-3}. Both temporal and spatial features of SF emission were studied following a two-photon excitation from the ground state. SF emission was observed to occur on the upper transition, along the direction of the collinear excitation pulses, as well as along directions in which both the upper and lower transitions satisfied phase-matching conditions. For the Rb system, the 5.2 μm emission was confirmed through studies of the integrated photon yield. The 5.2 μm SF evolved along all directions, while the 420 nm emission evolved along specific directions as determined by phase-matching conditions. In the Cs system, the upper transition wavelength was 876 nm ($6D$-$7P$) and suitable detectors were available for temporally resolved studies. It was established that in the forward direction the lower SF transition was triggered by the upper transition—a process termed "yoked SF." It was further observed that the lower transition had a small effect on the delay of the upper transition.

In this work, we present a study of SF on samples of laser-cooled Rb atoms for which $\tau_e < \tau_r$. The ground-state atom number N is varied from $\sim 10^7-10^9$. We use two traveling-wave excitation pulses near resonance with the $5S$-$5P$ and $5P$-$5D$ transitions, to transfer atoms from the ground state to the $5D$ excited state. The observed emissions are found to be sensitive to the delay time between the two excitation pulses. One limiting case is when the lower-transition pulse peaks before the upper-transition pulse, henceforth referred to as sequential excitation. Another limiting case occurs when the upper-transition pulse peaks before the lower-transition pulse; this case is referred to as stimulated Raman adiabatic passage (STIRAP) [27]. In both cases, a significant fraction of the ground-state population is transferred to the $5D$ state. Based on the photon yield observed on the $6P$-$5S$ decay channel and on simulations of the excitation process (see Fig. 4 below) we estimate a typical $5S \rightarrow 5D$ excitation efficiency of $\sim 50\%$. Therefore, for the data presented in this paper it is $N_{ex} \approx 0.5N$ (except for the outermost data points in the inset of Fig. 3, where N_{ex} is lower). The $5D$-$6S$ transition, at 5.2 μm, meets the conditions for SF, namely, that $\tau_r \ll T_2$ and $\tau_d < \tau_n = 241$ ns. We observe time-delayed triggered SF on the $6P$-$5S$ transition at 420 nm under conditions in which only the $5D$-$6P$ transition is expected to evolve through SF. The time delay of the 420 nm emission relative to the excitation pulses scales as $\sim N^{-1}$. The measured time delays are much smaller than expected for the case of cascade fluorescence, and agree with the expected time delay for the 5.2 μm SF. If the shape of the trapped sample is changed from a sphere to a cigar, we observe that the 420 nm emission changes from being isotropic to being strongly enhanced along the long axis of the sample. We compare the observed anisotropy with predictions based on a semiclassical treatment [2,28]. For the cigar-shaped cloud, the SF time delays are sufficiently short that the SF emission peak can be well distinguished from that of the incoherent cascade emission. We also find that triggered SF is dominant for STIRAP ordering of the excitation pulses,

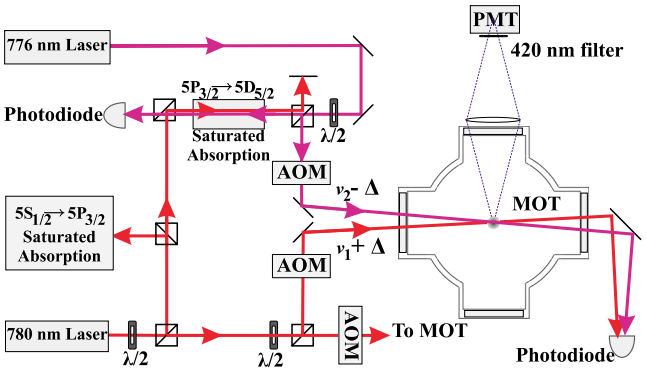

FIG. 2. (Color online) Diagram of experimental setup. SF emissions at 420 nm can be measured both perpendicular to and along the direction of the excitation pulses. (ν_1 denotes the frequency of the $5S_{1/2}, F=2 \rightarrow 5P_{3/2}, F=3$ transition, and ν_2 that of the $5P_{3/2}, F=3 \rightarrow 5D_{5/2}, F=4$ transition.)

and that cascade fluorescence is dominant in the case of sequential ordering of the excitation pulses. Related work in trapped atoms includes Ref. [29], where the efficiency of STIRAP excitation of the $5D$ level has been investigated. However, SF-like emissions were not observed in this work, presumably because the number of excited atoms N_{ex} was below threshold.

III. EXPERIMENTAL DETAILS

A schematic of the experimental setup is shown in Fig. 2. A portion of the light from a home-built grating-stabilized diode laser is locked to a crossover resonance ~130 MHz below the 780 nm $5S_{1/2}, F=2 \rightarrow 5P_{3/2}, F=3$ transition of ^{87}Rb. Light from this laser is amplified to approximately ~200 mW using an amplifier laser. Light from the amplifier laser is split up and sent through two dual-pass acousto-optical modulators (AOMs) operating near 80 MHz. One AOM is used to derive the beams for the magneto-optic trap (MOT) (~2 linewidths red-detuned with respect to the $5S_{1/2}, F=2 \rightarrow 5P_{3/2}, F=3$ transition). The other AOM generates the lower-transition excitation beam for the SF experiment (frequency ~20 MHz blue-detuned with respect to the $5S_{1/2}, F=2 \rightarrow 5P_{3/2}, F=3$ transition).

A separate home-built grating-stabilized external cavity diode laser (ECDL) is used to generate MOT "repumping" light at the $5S_{1/2}, F=1 \rightarrow 5P_{3/2}, F=2$ transition wavelength. Another ECDL is used to produce ~50 mW of 776 nm light. Beams derived from the locked 780 nm laser and the 776 nm laser are counterpropagated through a Rb vapor cell at room temperature. The inherently Doppler-free two-photon transition resonances into $5D_{5/2}$ hyperfine levels can be observed by measuring the absorption of 776 nm light in the Rb cell. The 776 nm laser is stabilized by means of side locking to the $5P_{3/2}, F=3 \rightarrow 5D_{5/2}, F=4$ absorption resonance. A dual-pass AOM, operating near 80 MHz, is used to prepare the upper-transition excitation beam for the SF experiment. In this excitation scheme, the 780 nm lower-transition excitation pulse is approximately 30 MHz blue-detuned with respect to the $5S_{1/2}, F=2 \rightarrow 5P_{3/2}, F=3$ transition, and the 776 nm upper-transition excitation pulse is equally red-detuned with respect to the $5P_{3/2}, F=3 \rightarrow 5D_{5/2}, F=4$ transition.

The repetition rate of the experiment is approximately 50 Hz. Typically, 10^8 atoms are loaded from a vapor cell into the MOT [30,31]. The trapping and repumping lasers are turned off in ~100 ns, and the magnetic-field gradient is turned off in ~100 μs. The excitation pulses are typically applied 500 μs after turn-off of the MOT magnetic field. The atom number is varied by changing the loading time of the MOT. We use a pair of circular anti-Helmholtz coils to produce spherical trapped-atom clouds of radius ~2 mm. Alternately, in some experiments we use a pair of racetrack-shaped coils to produce elongated cigar-shaped atom clouds with a long diameter of ~10 mm and an aspect ratio of 5:1. A high-speed photomultiplier tube (PMT) with a rise time of 4–5 ns, a 420 nm interference filter (~10 nm bandwidth) and a dc amplifier (350 MHz bandwidth) are used to measure the time-resolved emissions at 420 nm. Silicon photodiodes (~1 ns rise time) are used to record the excitation pulses.

A network of rf switches and a delay generator are used to drive the excitation pulses. The pulses have Gaussian spatial profiles that are larger than the cloud size in all cases. The typical full width half maxima of the spatial profiles are ~2 mm, and temporal durations are typically 200 ns. For the case of the cigar-shaped trap, the peak intensities of the excitation pulses are $I \approx 24 I_{sat}$ for the 780 nm beam and $I \approx 8 I_{sat}$ for the 776 nm beam, where I_{sat} are the respective saturation intensities averaged over the magnetic sublevels (7 mW/cm^2 for the 780 nm transition and 120 mW/cm^2 for the 776 nm transition). For the spherical trap, the intensities are $I \approx 10 I_{sat}$ for the 780 nm beam and $I \approx 3 I_{sat}$ for the 776 nm beam.

IV. RESULTS AND DISCUSSION

A. Time-dependence of emission signals

We first describe time-resolved measurements of the 420 nm emission on the transition $6P_{3/2} \rightarrow 5S_{1/2}$ along the long axis of cigar-shaped atom clouds. Each curve in Fig. 3 represents the emission intensity versus time for a distinct ground-state atom number N. The atom number N is varied by changing the loading time of the MOT. The steady-state MOT fluorescence is monitored using a calibrated photodetector. The number of atoms in the ground state N is determined from the measured photocurrent, the solid angle subtended by the detector, the total intensity of the MOT beams and the detuning of the MOT beams from resonance. It is assumed that the MOT fluorescence is isotropic.

It is evident in Fig. 3 that for large N two time-resolved peaks occur. The time delay of the second peak (peak 2) remains unchanged. We interpret peak 2 as being due to cascade fluorescence. To support this interpretation, we have modeled the level system shown in Fig. 1 using rate equations for atomic populations. In the simulation, a laser pulse

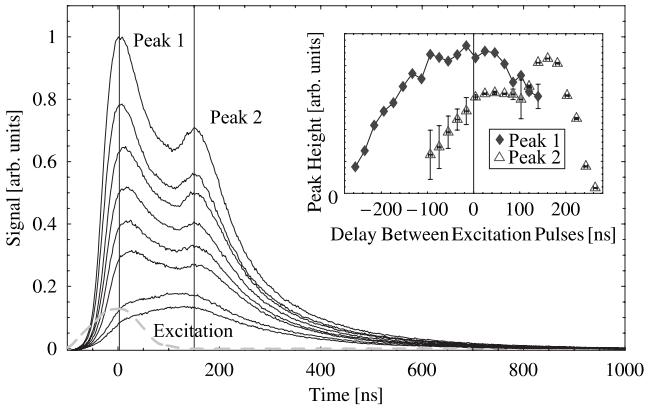

FIG. 3. Time-resolved SF detected along the long axis of cigar-shaped atom clouds for various ground-state atom numbers N. The excitation pulses are overlapped, and time $t=0$ corresponds to the center of the excitation pulses. The atom number N increases from the bottom to the top curve. The dashed curve indicates the time-dependence of the excitation pulses. The inset shows the height of the two maxima observed in the time-resolved emission signals (peak 1 and peak 2) for a fixed number of atoms, as a function of the delay time between the two excitation pulses. (Delay time <0 corresponds to STIRAP excitation pulse ordering, while delay time >0 corresponds to sequential excitation pulse ordering.)

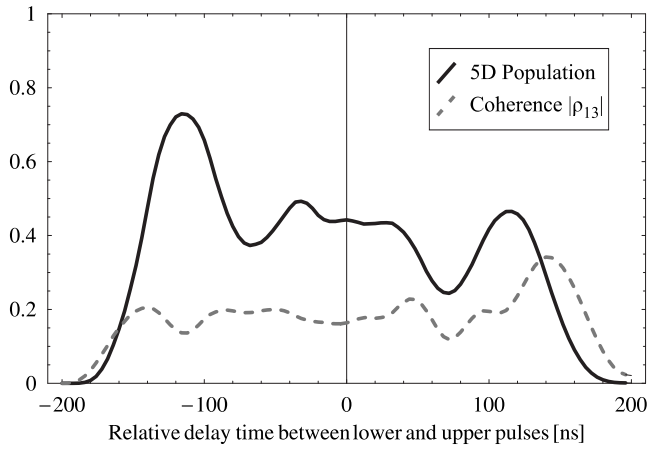

FIG. 4. Calculated $5D$ excitation probability (solid) and $5S$-$5D$ coherence (dashed) versus delay time between excitation pulses for typical experimental parameters. Negative delays correspond to STIRAP excitation.

with a Gaussian envelope (FWHM ~200 ns) excites atoms from the $5S$ to the $5D$ level. The simulation shows that the 420 nm emission resulting from uncorrelated decay peaks at a delay time of ~200 ns. This predicted delay of the cascade fluorescence peak matches the peak 2 in Fig. 3 reasonably well.

The first of the peaks in Fig. 3 (peak 1) shows the essential characteristic of SF, namely, a decreasing time delay with increasing N. In accordance with this interpretation it is also observed that peak 1 increasingly dominates peak 2 as N increases. For large atom numbers, the peak 1 practically coincides in time with the excitation pulses, shown as a dashed line in Fig. 3. This observation indicates that the $5D$ level is regeneratively pumped while the SF emission occurs [32]. The regenerative pumping will be further discussed in Sec. IV C.

The inset in Fig. 3 shows the peak heights of the time-resolved emissions as a function of the delay between the excitation pulses for a fixed atom number ($N \approx 3 \times 10^8$). Negative pulse delays correspond to STIRAP excitation, where the 776 nm pulse precedes the 780 nm pulse, while positive pulse delays correspond to sequential excitation. The SF emission in peak 1 is dominant in the STIRAP regime and a large part of the sequential regime. The cascade fluorescence (peak 2) dominates for sequential excitation-pulse ordering with pulse delays larger than about +100 ns.

Estimates based on Eq. (1), assuming the largest atom numbers available in our experiment, show that SF should occur on the $5D \rightarrow 6P$ transition, while conditions are below the SF threshold for the $6P \rightarrow 5S$ transition. Therefore, for the higher atom numbers in Fig. 3 SF on the $5D \rightarrow 6P$ transition is expected to rapidly populate the $6P$ level, leading to a rapid onset of 420 nm emission, as observed in peak 1 in Fig. 3. The 420 nm emission appears to be SF as well, as evidenced by the presence of two peaks in Fig. 3, the short duration of the emission peak 1 (which is of the order, or less than the $6P$ lifetime), and the high directionality of the 420 nm emission for cigar-shaped clouds (discussed in more detail in Sec. IV C). As the conditions in our experiment are below threshold for SF on the $6P \rightarrow 5S$ transition, the observed apparently superfluorescent emission on that transition must be attributed to triggered SF [24,25], that results from coherence between the $5S$ and $5D$ state amplitudes generated during excitation. To support this assertion further, we have numerically simulated the excitation process for a single atom, assuming typical experimental Rabi frequencies and taking the decay from the intermediate level into account. The results, shown in Fig. 4, indicate that over a wide range of pulse delays there is considerable build-up of $5D$ population as well as $5S$-$5D$ coherence. Therefore, from Fig. 4 we conclude that the ingredients necessary for triggered SF on the $6P \rightarrow 5S$ transition are present in our experiment. However, the simulation is for a single atom only and does not account for any cooperative phenomena. A theoretical model of cooperative decay occurring while the excitation pulses are still on, as evident in Fig. 3 for times $\lesssim 100$ ns, is beyond the scope of the present paper.

An analysis of the widths of the emission peaks in Fig. 3 is difficult to accomplish, since the peak widths are on the same order as the width of the excitation pulses and since peaks 1 and 2 are quite close to each other. Nevertheless, the rise time of peak 1 (which should be correlated with the pulse width) shows a decrease with increasing atom number, as expected for superfluorescent decay.

We have also obtained time-resolved emission curves for spherical atom clouds. While indications of SF are observed in this case as well (see Secs. IV B and IV C), it is generally difficult to observe SF and cascade fluorescence in a time-resolved manner, presumably because cascade and SF emissions have too much temporal overlap.

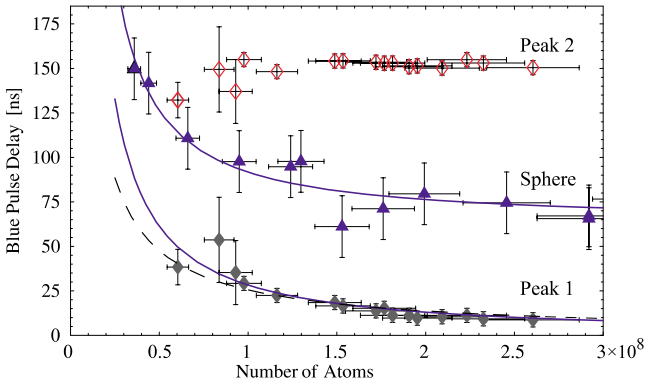

FIG. 5. (Color online) Delay time of SF vs number of atoms. The delays marked peak 1 (solid diamonds) and peak 2 (empty diamonds) correspond to temporally resolved peaks, as shown in Fig. 3, measured along the long axis of the cigar-shaped cloud. Delays for the spherical trap are shown with triangles. For the case of the cigar and the sphere, the experimental data are fitted with functions of the type $aN^{-x}+b$ with fit parameters a, b, and x, shown as solid lines. The fits show that the delays scale as the expected, with $x=(1.12\pm0.16)$ for the cigar and (1.17 ± 0.14) for the sphere, respectively. The offset b is zero for the cigar and ~70 ns for the sphere. The dashed line shows the predicted 5.2 μm delay, calculated on the basis of Eq. (1) using measured cloud parameters. Numerical simulations for cascade fluorescence suggest that peak 2 should occur at 174 ns.

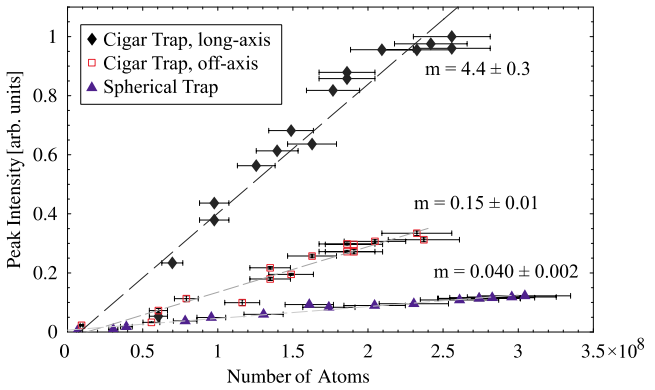

FIG. 6. (Color online) Peak intensity as a function of number of trapped atoms for the long axis of the cigar-shaped trap, short axis of the cigar-shaped trap, and for a spherical trap. The graph for the case of the long axis of the cigar-shaped trap has been scaled down by a factor of 10. The slopes m based on linear fits are indicated.

B. Delay times of emission peaks

In the following, we compare the time delays of the emission peaks observed for both cigar-shaped and spherical atom clouds. Figure 5 shows the time delays as a function of N for peak 1 (solid diamonds) and peak 2 (empty diamonds) for observation along the long axis of the cigar-shaped cloud. The delays are measured with respect to the peak of the excitation pulses (with 780 and 776 nm pulses temporally overlapped). A fit to the data for peak 1 (solid line) establishes that the SF emission exhibits the expected N^{-1} variation, with no fit offset. The dashed line shows the expected SF delay for 5.2 μm emission, for the same range of N, calculated using Eq. (1) based on the measured trap parameters. Although the two curves are in excellent agreement, we note that there are systematic uncertainties with the measured trap parameters, at the level of $\pm10\%$. Nevertheless, it is clear that the predicted time delay for the 5.2 μm occurs on the same time scale as the 420 nm SF. This indicates that the 420 nm emission is triggered by the presence of the 5.2 μm emission, confirming the results in Ref. [24]. The data also shows that there is no variation in the delay time for peak 2, consistent with expectations for cascade fluorescence. The discrepancy between the observed delay ($\approx$150 ns) and the predicted delay for cascade fluorescence (174 ns for an excitation FWHM of 114 ns) can be attributed to the uncertainty in the degree of overlap between excitation pulses.

Similar data for the time delay of emission from the spherical trap (triangles) is also shown in Fig. 5. A fit (solid line) establishes that the emission exhibits a N^{-1} dependence, indicating superfluorescent decay. The emission delay for the spherical cloud is considerably longer than for the case of the cigar-shaped cloud (peak 1). We attribute this difference to the fact that for the spherical cloud the value of μ and the atom density are lower than for the cigar-shaped cloud. For spherical atom clouds, we cannot resolve the SF emission from the cascade emission over the entire accessible range of N. The fact that for spherical clouds the SF and cascade emissions blend into each other may explain the fit offset of ~70 ns for the case of the spherical cloud, apparent in Fig. 5.

C. Peak intensities of SF emission

Finally, we describe the observed trends for the peak intensities of the SF emission. Figure 6 shows the peak intensities of the SF emission, measured by the PMT, as a function of the number of ground-state atoms N. For the cigar-shaped cloud, the SF signal at 420 nm was measured along both the long and short axes of the cloud. The peak intensities are determined by accounting for the solid angles subtended by the effective aperture of the detection apparatus. Fits to the data in Fig. 6 show that the SF peak intensities vary linearly as a function N for both the long and short axes of the cigar-shaped cloud, as well as for the spherical cloud. For pure SF, assuming instantaneous excitation, a quadratic dependence of the peak intensity on N would be expected. However, the presence of SF emission during the excitation pulse in Fig. 3 strongly suggests that the excitation pulse duration is comparable with the effective excited-state lifetime and that the $5D$ level is regeneratively pumped in our experiment. As a result, we would expect the 420 nm peak intensity to show a linear dependence on N, as the evolution of SF is continuously interrupted by repeated population transfer to the $5D$ level. The observed linear scaling of the peak intensity with N is consistent with an earlier experiment involving regenerative pumping [32], where the peak intensity was also observed to be proportional to N.

Figure 6 shows that the slopes of straight-line fits for the peak intensity for the sphere and along the short axis of the

cigar-shaped cloud are comparable. For the case of the sphere, the average SF peak intensity measured both parallel and perpendicular to the excitation beams are the same, within experimental error. Thus, the emission from the spherical cloud is essentially isotropic. This is consistent with the expectation for a sample with a high Fresnel number of $\mathcal{F}\sim 7500$, which would have $\sim\mathcal{F}^2$ spatial emission modes. The photon yield of the 420 nm emission extrapolated over the whole sphere is comparable to the atom number N in the ground state, suggesting that the dominant channel for deexcitation of the $5D$ level is SF via the intermediate $6P$ level.

The SF emission is found to be highly anisotropic for the cigar-shaped cloud. Along the long axis of the cigar-shaped cloud, the peak intensity is found to be ~29 times higher than along the short axis. For detection along the long axis, the excitation beams were at an angle of 0.068 ± 0.008 rad and essentially all of the SF emission was concentrated within a narrow cone with a full angle of 0.051 ± 0.005 rad, centered between the directions of the two excitation pulses. The ratio of μ factors for the long and short axes of the cigar-shaped cloud (recorded at the same density) is 4.8 ± 0.9, while the respective ratio of slopes in Fig. 6 is (29 ± 2.8).

All our experimental observations from Fig. 6 together suggest that the SF intensity scales as μ^2N. A semiclassical treatment of the case of SF with instantaneous excitation (pure SF) [2,28] shows that the peak height should scale as $(\mu N)^2$, where (μN) represents an effective dipole moment. For regenerative pumping, one may expect an SF intensity $\propto\mu N$. Sources of this discrepancy are not well understood. We speculate that our experiment may have operated in a transitional regime. This suspicion is supported by a few data sets that have shown a nonlinear dependence of the SF intensity on N. (We do not show these data because they were not typical and could not be reproduced.)

We have considered the effect of radiation trapping as a possible source of these discrepancies. This effect can be ruled out based on several estimates. Reference [18] described an experiment carried out at densities of $\sim 10^{14}$ cm^{-3} in which the lifetime of the excited state (~5 ns) was effectively extended to ~1 μs due to radiation trapping. This effect allowed SF pulses to evolve on time scales that were much longer than the lifetime. In contrast, our work was carried out at densities of $\sim 10^{11}$ cm^{-3}. Under these conditions, the optical depth (αL) of the sample for the 780 nm transition can be estimated to be ~5. Here, α is the absorption coefficient and L is the length of the sample. In this case, although radiation trapping can have a significant effect on the 780 nm transition, it is not significant for the SF pulses that evolve on the 5.2 μm and 420 nm transitions. This is because the line strengths (and corresponding absorption coefficients) for these transitions are 10–20 times smaller than the corresponding parameters of the 780 nm transition. In addition, in our work the time scale on which the SF pulses evolve on these transitions (~100 ns) is significantly shorter than the lifetimes of the $5D$-$6P$ (~650 ns) and $6P$-$5S$ transitions (~350 ns), suggesting that multiple absorption events can be ruled out.

The small signal gain for SF (which applies at the time of SF initiation) can be estimated from Ref. [33] as $\alpha L = 2T_2/\tau_r$. For typical experimental conditions, the gain of the upper (5.2 μm) transition is ~200, consistent with rapid deexcitation of the $5D$ level via SF. Under these conditions, the $6P$ state is initially unpopulated. As a result, no radiation trapping is expected on the upper transition. For the lower (420 nm) transition, the small signal gain is small (~1). We find that SF evolves on a time scale (~100 ns) that is smaller than the upper level lifetime only because it is triggered by the evolution of SF on the upper transition. Therefore, this estimate also rules out radiation trapping. A more formal analysis based on Holstein's results for a cylindrical geometry [34,35] also suggests that the effective lifetime of the SF transitions is not enhanced because of radiation trapping.

D. Discussion

In summary, the presence of triggered SF on the 420 nm transition is strongly supported by several observations. First, N is significantly smaller than the threshold number for SF on the 420 nm transition. Second, the predicted delay time for SF on the 420 nm transition, in the absence of any triggering process, can be estimated to be up to ten times longer than the observed time delays. In addition, the predicted delay time for 5.2 μm SF coincides with the measured 420 nm SF delay time. Finally, for the case of the cigar-shaped sample excited by the 780 and 776 nm pulses at a small angle of 0.068 ± 0.008 rad, the peak SF intensity at 420 nm was recorded over a cone angle of 0.051 ± 0.005 rad, centered between the directions of the two excitation pulses. This is consistent with the expected direction for phase-matched emission, as observed for triggered SF in Ref. [26]. This work also shows that the triggered SF emission on the 420 nm transition is associated with coherent excitation.

V. CONCLUSIONS

We have reported an observation of triggered SF emissions from a sample of trapped atoms. The atom number used in these experiments is substantially lower than in previous studies of SF. The SF emission shows an enhancement in intensity when the shape of the cloud is changed from a sphere to a cigar. Time-resolved measurements of the emission also show that SF is dominant in the STIRAP regime of the two-photon excitation, and that cascade fluorescence sometimes dominates in the case of sequential excitation.

In future studies in cold atoms, it could be investigated if the expected SF cascade emissions at 5.2, 2.7, and 1.4 μm occur in the presence of incoherent excitation. Detection of time-resolved signals with adequate signal to noise ratio at

these wavelengths would constitute the main experimental challenge. Applications of this work could extend to studies of dephasing processes, such as interatomic interactions, in cold atoms. Other applications could relate to Bose-condensed samples that typically have low atom numbers and verification of predicted statistical properties for spherical samples [36].

ACKNOWLEDGMENTS

This work is supported by Canada Foundation for Innovation, Ontario Innovation Trust, Photonics Research Ontario, Natural Sciences and Engineering Research Council of Canada, NSF Grant Nos. PHY-0114336 (FOCUS) and PHY-0555520, York University and the University of Michigan.

[1] M. Gross and S. Haroche, Phys. Rep. **93**, 301 (1982).
[2] N. E. Rehler and J. H. Eberly, Phys. Rev. A **3**, 1735 (1971).
[3] F. Haake, H. King, G. Schröder, J. Haus, R. Glauber, and F. Hopf, Phys. Rev. Lett. **42**, 1740 (1979).
[4] R. J. Glauber and F. Haake, Phys. Rev. A **13**, 357 (1976).
[5] M. G. Raymer and I. A. Walmsley, Prog. Opt. **28**, 181 (1990).
[6] R. H. Dicke, Phys. Rev. **93**, 99 (1954).
[7] D. Schneble, Y. Torii, M. Boyd, E. W. Steed, D. E. Pritchard, and W. Ketterle, Science **300**, 475 (2003).
[8] H. M. Gibbs, Q. H. F. Vrehen, and H. M. J. Hikspoors, Phys. Rev. Lett. **39**, 547 (1977).
[9] N. Skribanowitz, I. P. Herman, J. C. MacGillivray, and M. S. Feld, Phys. Rev. Lett. **30**, 309 (1973).
[10] Q. H. F. Vrehen, H. M. Gibbs, and R. Bonifacio, *Dissipative Systems in Quantum Optics* (Springer-Verlag, Berlin, 1982), pp. 111–147.
[11] D. J. Heinzen, J. E. Thomas, and M. S. Feld, Phys. Rev. Lett. **54**, 677 (1985).
[12] M. F. H. Schuurmans, Opt. Commun. **34**, 185 (1980).
[13] J. J. Maki, M. S. Malcuit, M. G. Raymer, R. W. Boyd, and P. D. Drummond, Phys. Rev. A **40**, 5135 (1989).
[14] R. Bonifacio and L. A. Lugiato, Phys. Rev. A **11**, 1507 (1975).
[15] D. Polder, M. F. H. Schuurmans, and Q. H. F. Vrehen, Phys. Rev. A **19**, 1192 (1979).
[16] F. T. Arecchi and E. Courtens, Phys. Rev. A **2**, 1730 (1970).
[17] A. Kumarakrishnan, S. Chudasama, and X. L. Han, J. Opt. Soc. Am. B **22**, 1538 (2005).
[18] A. Kumarakrishnan and X. L. Han, Phys. Rev. A **58**, 4153 (1998).
[19] E. Arimondo, M. Inguscio, and P. Violino, Rev. Mod. Phys. **49**, 31 (1977).
[20] J. E. Sansonetti, J. Phys. Chem. Ref. Data **35**, 301 (2006).
[21] T. T. Grove, V. Sanchez-Villicana, B. C. Duncan, S. Malecki, and P. L. Gould, Phys. Scr. **52**, 271 (1995).
[22] J. Marek, J. Phys. B **12**, L229 (1979).
[23] C. M. Bowden and C. C. Sung, Phys. Rev. A **18**, 1558 (1978).
[24] A. I. Lvovsky, S. R. Hartmann, and F. Moshary, Phys. Rev. Lett. **82**, 4420 (1999).
[25] A. I. Lvovsky, S. R. Hartmann, and F. Moshary, Phys. Rev. Lett. **89**, 263602 (2002).
[26] J. H. Brownell, X. Lu, and S. R. Hartmann, Phys. Rev. Lett. **75**, 3265 (1995).
[27] U. Gaubatz, P. Rudecki, S. Schiemann, and K. Bergmann, J. Chem. Phys. **92**, 5363 (1990).
[28] L. Allen and J. H. Eberly, *Optical Resonance and Two-level Atoms* (Dover, New York, 1987).
[29] W. Suptitz, B. C. Duncan, and P. L. Gould, J. Opt. Soc. Am. B **14**, 1001 (1997).
[30] C. Monroe, W. Swann, H. Robinson, and C. Wieman, Phys. Rev. Lett. **65**, 1571 (1990).
[31] E. L. Raab, M. G. Prentiss, A. E. Cable, S. Chu, and D. E. Pritchard, Phys. Rev. Lett. **59**, 2631 (1987).
[32] M. Gross, C. Fabrem, P. Pillet, and S. Haroche, Phys. Rev. Lett. **36**, 1035 (1976).
[33] R. Friedberg and S. R. Hartmann, Phys. Lett. **37A**, 285 (1971).
[34] T. Holstein, Phys. Rev. **72**, 1212 (1947).
[35] T. Holstein, Phys. Rev. **83**, 1159 (1951).
[36] S. Prasad and R. J. Glauber, Phys. Rev. A **31**, 1583 (1985).